Research Square

Preprints are preliminary reports that have not undergone peer review.
They should not be considered conclusive, used to inform clinical practice,
or referenced by the media as validated information.

Magnetically Actuated Helical Microrobots Enabling Ultrasound-Free Precision Fragmentation of Lens Nuclei in Cataract Surgery

Lin Ding

linding@csu.edu.cn

Changsha Aier Eye Hospital, Aier School of Ophthalmology, Central South University, Changsha, Hunan, China.

Zhelin Li

Changsha Aier Eye Hospital, Aier School of Ophthalmology, Central South University, Changsha, Hunan, China.

Yingying Wei

Changsha Aier Eye Hospital, Aier School of Ophthalmology, Central South University, Changsha, Hunan, China.

Qiongyan Tang

Changsha Aier Eye Hospital, Aier School of Ophthalmology, Central South University, Changsha, Hunan, China.

Weitao Song

The Xiangya Hospital, Central South University

Xinjian Fan

Jiangsu Provincial Key Laboratory of Advanced Robotics, School of Mechanical and Electric Engineering, Soochow University

Article

Keywords: Cataract surgery, Microrobots, Lens fragmentation, Composite Magnetic Drive System

Posted Date: March 8th, 2026

DOI: https://doi.org/10.21203/rs.3.rs-8761917/v1

License: This work is licensed under a Creative Commons Attribution 4.0 International License.
Read Full License

Additional Declarations: There is no conflict of interest

Abstract

Despite its status as the gold standard for cataract surgery, phacoemulsification carries inherent risks associated with ultrasonic energy application, including intraoperative complications (e.g., posterior capsule rupture) and a steep surgical learning curve. To address these limitations, this study presents a magnetically actuated composite micro-robotic system engineered specifically for lens fragmentation. Utilizing a human-robot interaction (HRI) module for external teleoperation, we experimentally evaluated the locomotion capabilities of individual helical magnetic microrobots (Helixbots) within a viscoelastic medium and ex vivo porcine lens. Results demonstrated the helixbots' capability for multidirectional navigation and achieved partial fragmentation of the lens nucleus. This microrobotic platform establishes a foundation for ultrasonic energy-free cataract surgery, offering enhanced procedural safety through the absence of ultrasonic energy, improved predictability, and real-time controllability. Crucially, this work provides preliminary experimental validation of ultrasonic energy-free lens fragmentation, a pivotal surgical step, thus demonstrating a promising and transformative strategy with significant potential clinical value.

1. Introduction

Cataracts represent the leading global cause of blindness and a primary contributor to vision impairment[1]. characterized by progressive visual decline, image blurring, photophobia, glare, visual field deficits, and dyschromatopsia. Without timely intervention, cataracts inevitably cause blindness that severely diminishes quality of life and correlates with reduced life expectancy [2,3]. Surgery remains the only proven and effective clinical treatment for cataracts at present[4]. In the 1960s, Charles Kelman pioneered phacoemulsification technology. This approach employs high-frequency ultrasonic probes to fragment and emulsify the lens nucleus, reducing incision size from 11 mm to sub-3-mm levels. Combined with the foldable intraocular lens implantation technology, it significantly reduces tissue damage and enables sutureless wound healing. It has now become the mainstream surgical procedure internationally. Nevertheless, significant unresolved limitations persist: Phacoemulsification demands exceptional surgical skill, requiring precise control of ultrasonic energy release and operative time—critical factors directly linked to postoperative corneal edema, endothelial cell loss, and compromised visual outcomes [5–8]; inexperienced surgeons risk perforating the capsule, potentially causing sight-threatening complications like zonular dehiscence or vitreous prolapse; thus, surgical success hinges entirely on operator expertise, establishing steep learning curves with prolonged training requirements that exacerbate global healthcare disparities, particularly in resource-limited regions lacking high-quality surgical capacity.

Although femtosecond laser-assisted cataract surgery (FLACS) automates capsulorhexis and nuclear pre-fragmentation[9]—demonstrating superior predictability, precision, and reproducibility —it fails to address the core limitation: dependence on manual phacoemulsification for lens nucleus disassembly[1]. This fundamental constraint perpetuates inefficiency, elevated intraoperative risks, high complication

rates, and persistent training barriers in cataract surgery. Therefore, developing innovative lens nucleus processing systems is imperative. Eliminating ultrasound energy dependence while transcending manual precision barriers will minimize complication risks, compress surgical training demands, catalyze a safety-centered paradigm shift in cataract surgery, and advance global equity in ophthalmic care accessibility.

Achieving precise controllable medical interventions via micro-nano robots within the human body remains a paramount challenge in biomedical engineering[10,11]. Recent microrobotics advances have catalyzed innovations across micromanufacturing, precision medicine, and bioengineering[12]. Crucially, magnetically actuated microrobots exhibit exceptional tissue penetrability, wireless controllability, high-fidelity manipulation, and biocompatibility, establishing their transformative potential as intraocular surgical actuators[13,14]. The synergistic integration of microrobotic flexibility with external magnetic field guidance enables precise intraocular maneuvers—delivering unprecedented surgical solutions for cataract intervention. Despite these advantages, significant technical bottlenecks persist in complex intraocular environments: Specifically, in low-Reynolds-number biological fluids where microrobotic motion mechanisms fundamentally diverge from macroscale dynamics, high-viscosity intraocular environment drastically reduce propulsion efficiency; Although existing studies have achieved basic unidirectional translation in the vitreous via magnetic/optical actuation, yet failed to achieve multi-degree-of-freedom manipulation. Furthermore, the absence of real-time tracking and closed-loop feedback systems impedes dynamic pose calibration and surgical safety assurance. Critically, current research remains confined to simplistic motions in the low-density vitreous[15–17], while microrobotic operations within the lens lack substantive breakthroughs.

Herein, we introduce a magnetically controlled microrobotic platform engineered specifically for lens fragmentation in cataract surgery. This system enables ultrasound-free lens fragmentation via precise external magnetic field manipulation of helixbots. Building upon our established theoretical framework for magnetic micro-robot control in biological fluids, we implemented an innovative hybrid electromagnetic-permanent magnet drive system. Using real-time human-in-the-loop control, helixbots achieved targeted propulsion, steering, and lens fragmentation in ex vivo porcine. Critically, by exploiting differential mechanical properties (elasticity, toughness) between the lens nucleus and surrounding capsule, helixbots' structural and kinematic parameters dynamically adapt to selectively fragment nuclear tissue while preserving capsular integrity with no observable tearing. Furthermore, autonomous path navigation was demonstrated in a synovial fluid-mimicking viscoelastic medium. Collectively, the helixbots platform overcomes fundamental energy-dependent limitations of traditional phacoemulsification, establishing a transformative surgical paradigm characterized by ultrasound-free tissue preservation, minimized intraoperative risks, and predictable robotic operations.

2. Results and Discussion

Fabrication of Microrobot and Composite Magnetic Drive System

The fabrication of the helixbots involves two functionally distinct modular components: a cylindrical magnetic drive module serving as the actuation unit, and a helical biocompatible body module designed for tissue interaction. The magnetic drive module was fabricated using high-permeability magnetic sphere composites to ensure optimal responsiveness to external magnetic fields, while the body module was constructed from medical-grade biocompatible photopolymer resin (Dental SG Resin, Formlabs Inc., Somerville, MA, USA). The body module incorporates an architecturally optimized spiral structure with progressive pitch variation - featuring coarser helical grooves at the proximal end transitioning to finer distal grooves - specifically engineered to achieve efficient lens fragmentation (Fig. 1A). For precise fabrication, we employed additive manufacturing techniques combining stereolithography (SLA) for the polymeric components and selective laser melting (SLM) for metallic elements. Nickel-iron alloy was selected for the magnetic segments due to its favorable ferromagnetic properties. The magnetic segments are cylindrical, with the radius of the base circle being 0.75 mm and the height of the cylinder being 2 mm. The surface of the magnetic segments encapsulated with medical glue to ensure its biocompatibility. Particular attention was paid to maintaining precision and structural integrity throughout the assembly process. The characterization of the assembled robot under a microscope is shown in Fig. 1D, with a width of approximately 2 mm and a length of about 4 mm.

To achieve precise control of magnetic fields for microrobot manipulation, we developed an electromagnetic actuation system based entirely on electromagnetic coils. This system generates programmable magnetic field vectors with arbitrary three-dimensional orientations, enabling omnidirectional rotational control of magnetic microrobots. The setup comprises stationary electromagnetic coils operated via current control, secured between upper and lower base plates on a dedicated platform (Fig. S1). Each electromagnet unit consists of two parallel coils wound with 0.4 mm diameter enameled wire, resulting in a combined parallel resistance of 4.4 Ω. At a rated operating voltage of 25 V, the system generates a peak magnetic flux density of 16 mT in the central workspace.

Each coil incorporates soft magnetic material to amplify the generated magnetic field. The workspace is a 40 × 40 × 40 mm^3 cube, and the coils employ a parallel inner-outer ring configuration to reduce resistance and increase current. Two power supplies (eTM-6030, TOMMENS) and six power amplifiers (OPA541, Texas Instruments) were connected to an eight-channel DAQ card (PCI-6733, National Instruments) for control signal input. To mitigate thermal fluctuations that could impair the magnetic field generation, water-cooling pipes were wound around the interior and exterior of the coils, with water pumps providing active heat dissipation. This thermal management system maintained a stable operating temperature of 24°C.

Figure 1b presents the conceptual framework of the helixbot platform for lens nucleus fragmentation in human cataract surgery, wherein the microrobot is implanted intralenticularly and directly controlled via a composite magnetic drive system integrated with a collaborative robotic interface. Surgeons manipulate the control handpiece to navigate predefined intraocular trajectories and execute fragmentation through human-machine interaction, while the surgical imaging system captures real-time pose tracking data using high-precision stereoscopic cameras. This information feeds into vision-based closed-loop control

for trajectory tracking, enabling autonomous navigation algorithms to dynamically optimize surgical paths.

To optimize helixbots for intraocular surgery, we developed magnetic actuation strategies that enhance propulsive speeds and environmental adaptability to meet functional demands within the lens capsule (Fig. 1D). We implemented three distinct field modalities: rolling, rotating, and conical magnetic fields. By precisely controlling three-dimensional magnetic field vectors, we overcome the directional limitations of traditional single-field sources. For instance, applying a rolling magnetic field enables rapid robot translation—particularly effective for traversing lenses several times the robot's diameter with rough surfaces. Applying a rotating magnetic field induces spiral propulsion in the helixbot; this mode requires no significant operational space, enabling efficient maneuvering within the confined lens capsule environment for nuclear splitting operations. Furthermore, conical magnetic fields generate swing-and-turn maneuvers, enhancing robot-lens interaction to achieve rapid, precise cutting.

Magnetic control theory of micro-robots in Biological Fluids

Magnetic microrobots in biofluid are governed by the interplay of hydrodynamic forces, gravi- tational forces, and the propulsive forces generated by their helical rotation. According to the scallop theorem for low Reynolds number hydrodynamics (Re $\ll$ 1), inertial forces are negligible. Consequently, the microrobots instantaneously achieve terminal velocity where the viscous drag (Fd) precisely counterbalances the driving forces. The governing equilibrium equation for translational motion is described as:

$$F_{prop} = F_d \quad (1-1)$$

Here, Fprop denotes the propulsive force generated by the rotation of the helical structure driven by the rotating external magnetic field. Based on Resistive Force Theory (RFT), this force arises from the anisotropic drag on the helical filament and is expressed as:

$$F_{prop} = (\xi_{\perp} - \xi_{\parallel})\sin\theta\cos\theta \cdot R \cdot L \cdot \omega \quad (1-2)$$

In this expression, ω represents the angular velocity of the microrobot, R and L denote the radius and total filament length of the helix respectively, θ is the helix pitch angle, while $\xi_{\perp}$ and $\xi_{\parallel}$ correspond to the drag coefficients perpendicular and parallel to the helical filament.

The opposing viscous drag (Fd) exerted by the biofluid is described by Stokes' law:

$$F_d = 6\pi\eta r v \quad (1-3)$$

where r represents the hydrodynamic radius of the robot, η is the dynamic viscosity of the fluid, and v is the forward velocity.

Vertical Forces: In the vertical direction, the microrobot is subject solely to the gravitational force (Fg) and the buoyant force (Fb). The gravitational force acting on the robot is defined as:

Fg = ρrobotVg (1–4)

where ρrobot is the density of the microrobot, V is its volume, and g is the gravitational acceleration. Simultaneously, the microrobot experiences an upward buoyant force exerted by the displaced fluid:

Fb = ρfluidVg (1–5)

where ρfluid represents the density of the surrounding medium. The net vertical force (Fnet vertical), which determines the sedimentation behavior, is given by the difference between these two forces:

Fnet vertical = Fg — Fb = (ρrobot — ρfluid)Vg (1–6)

Velocity Derivation: By substituting the expressions for Fprop and Fd into the horizontal equilibrium equation (Fprop = Fd) and isolating the velocity term, we derive the theoretical forward velocity v of the microrobot:

$$v = \frac{(\xi_{\perp} - \xi_{\parallel}) \sin\theta \cos\theta \cdot R \cdot L}{6\pi\eta r}\omega \qquad (1\text{-}7)$$

This derivation establishes the linear relationship between the input angular velocity (ω) and the output linear velocity (v), providing a fundamental theoretical framework for the motion control of intraocular microrobots.

Design of the Lens Surgery System with an Integrated Human-Machine Interaction Platform

We further developed a cataract nucleus fragmentation surgical robot system. The complete robotic surgical system comprises three integrated modules (Fig. 2B): a magnetically actuation surgical module for procedure execution, a data processing module for real-time signal processing and transmission, and a human-computer interaction module for outputting signals under operator control. Initially, a main incision and a side incision were created at the limbus, followed by injection of a viscoelastic agent into the anterior chamber. After performing preliminary cataract surgical steps, including continuous curvilinear capsulorhexis and hydrodissection, an ophthalmic instrument tip was used through the main incision into the viscoelastic-filled anterior chamber to implant the helixbots into the lens. The helixbots was then activated to move and perform operations according to preset parameters. Figure 2A depicts the positioning of the helixbot within the lens substance. Upon activation of the magnetic driving system, a camera was employed to observe and record the movement trajectory of the magnetically controlled robot within the lens and its interaction with surrounding lens tissue.

We constructed the human-computer interaction module using a computer integrated with LabVIEW software, enabling program computation and graphical rendering of the interaction interface. The system employs an NI eight-channel data acquisition board (NI-6733) to relay control signals from the host computer to four power amplifiers. These amplifiers connect to a power supply and

electromagnetic coils, distributing the amplified control signals across eight channels to individual coils. Independent voltage regulation for each coil facilitates precise magnetic field manipulation. The coordinated activation of these coils generates a non-uniform magnetic field that propels the helixbot, enabling three-dimensional trajectory execution within a defined spatial volume.Primary operational control is achieved via a handheld controller featuring dual joysticks, which independently modulate the x-, y-, and z-axis components of spatial vectors. Supplementary buttons allow real-time adjustment of input voltage magnitude. Figure 2C schematizes the micro magnetic-driven robot's human-computer interaction platform architecture. The three-dimensional motion control program interface (Fig. S2) permits user-defined modification of clinically relevant parameters, including magnetic amplitude, actuation frequency, duty cycle, and motion modes.

The magnetic drive system employs real-time positional feedback and instantaneous velocity computations to determine requisite current values for each electromagnetic coil through a control box interfaced with the host computer. This enables generation of a directional magnetic field that propels the magnetically actuated helixbot along predefined trajectories. An overhead optical tracking system continuously captures the helixbot's spatially resolved positional coordinates (x, y, z axes). Through adaptive binarization processing coupled with the Meanshift algorithm, the system achieves robust target localization of the helixbot. This methodology maintains targeting precision despite environmental disturbances, ensuring reliable system operation.

Characterization of Controllable Motion in Magnetically Actuated Microrobots

Precise intraoperative motion control of helixbots enhances adaptive navigation in complex intraocular surgical environments—a critical capability for clinical translation. To this end, we performed in vitro kinematic characterization of the helixbot within ophthalmic viscoelastic media. Quantitative analysis of propulsion and rotational velocities under varying magnetic field parameters advances fundamental understanding of microrobotic dynamic control, expanding applicability in intricate intraocular procedures.

As illustrated in Fig. 3, manual controller operation enables multidirectional positioning of the helixbot within viscoelastic material. Through modulation of magnetic field intensity and frequency, we regulated the propulsion and rotational velocities of the helixbot, establishing controlled locomotion capabilities. Precessional motion ensures that the helixbot can navigate along surgical pathways and perform cutting operations within the lens during cataract procedures. During propulsion velocity testing in a viscoelastic medium at an amplitude of 8 A/m, controllable directional motion of the helixbots was achieved at a frequency of 6 Hz. Subsequent measurements of propulsion velocity were conducted at frequencies ranging from 6 to 11 Hz. As shown in Fig. 3A, the average propulsion velocity reached 0.267 ± 0.025 mm/s at 6 Hz and increased to 0.311 ± 0.025 mm/s at 10 Hz. However, at 11 Hz, the velocities of the helixbots in the viscoelastic medium decreased to 0.243 ± 0.046 mm/s. Optimal and stable mobility was maintained between 7 and 10 Hz.

Under constant frequency conditions (8 Hz) (Fig. 3B), we systematically investigated the correlation between magnetic field intensity and propulsion velocity. At field amplitudes of 5–6 A/m, the helixbots exhibited propulsion velocities of 0.246 ± 0.044 mm/s and 0.254 ± 0.027 mm/s in the viscoelastic medium, respectively. Notably, within the amplitude range of 7–9 A/m, the helixbots maintained higher velocities, peaking at 0.306 ± 0.016 mm/s at 8 A/m. However, when the amplitude exceeded 10 A/m, we observed a significant decrease in the average propulsion velocity of the helixbots. These data indicate that the optimal control parameters for rapid navigation of helixbots in ophthalmic viscoelastic environments lie within the combined ranges of 7–9 A/m amplitude and 7–9 Hz frequency. Beyond thresholds of 10 A/m or 10 Hz, degraded locomotive capability indicates phase lag between microrobot orientation and magnetic field rotation, precipitating precipitous decline in propulsion efficiency.

Beyond the propulsion motion of the robot, we investigated the rotational characterization of the helixbots in viscoelastic medium to address the critical clinical requirement for multidirectional lens fragmentation. Systematic evaluation of magnetic field parameters revealed frequency- and intensity-dependent rotational behavior. At an amplitude of 8 A/m, the helixbots achieved initial controllable rotation at 5Hz, demonstrating an average rotational velocity of 50.31 ± 7.46°/s (mean ± SD)(Fig. 3C). Progressive frequency escalation from 5 Hz to 10 Hz yielded continuous rotational acceleration, reaching 252.89 ± 42.47°/s at 9 Hz and 490.19 ± 91.85°/s at 10 Hz. This positive correlation was accompanied by progressively increasing measurement variability, suggesting decreasing rotational stability at higher frequencies. Complementary 8 Hz testing (Fig. 3D) established that a minimum field intensity of 5 A/m was required to initiate rotation. Across the tested intensity range of 5–11 A/m, rotational velocity demonstrated amplitude dependence, plateauing between 6–8 A/m. The condition at 8 A/m produced optimal rotational stability (141.41 ± 7.70°/s), while an intensity of 10 A/m achieved a higher rotational velocity (248.46 ± 57.90°/s) but with significantly reduced control precision compared to the 6–9 A/m range.

Collectively, these findings define distinct operational regimes that balance rotational speed and control stability for intraocular surgical navigation. Figure 3G demonstrates linear propulsion and directional steering of helixbots within the viscoelastic medium using a handheld controller (Movie S1 and S2), while simultaneous surface rolling motion is achieved atop the medium at higher velocities (Movie S3).

The time-lapse images in Fig. 3E and 3F demonstrate controlled trajectories of Helixbots within the viscoelastic medium (Movie S4 and S5), with velocity exhibiting direct correlation to the rotational frequency and amplitude of the applied magnetic field. At 4 A/m amplitude, peak velocity of 0.725 mm/s occurs at 7 Hz (increasing from 0.2 mm/s at 1 Hz). At 6 A/m, peak velocity reaches 1.124 mm/s at 8 Hz (rising from 0.2 mm/s at 1 Hz). At 8 A/m, peak velocity achieves 1.364 mm/s at 8 Hz (growing from 0.2 mm/s at 1 Hz). Beyond these frequency optima, we observe progressive velocity degradation with further frequency increases, culminating in complete motion cessation.

Controlled Maneuvering and Lens Cutting within the Porcine Lenses

While magnetically controlled micro/nanorobots offer distinct advantages for precision ophthalmic surgery, their deployment in complex intraocular environments poses substantial challenges. The fundamental physics governing microrobot motion in low-Reynolds-number biological fluids diverges markedly from macroscopic dynamics. Elevated viscosity in ocular tissues significantly impedes propulsion efficiency. Although prior studies established basic translational motion capabilities in the vitreous using magnetic/optical actuation, achieving true multi-degree-of-freedom (MDoF) control remains unresolved. Current research primarily demonstrates elementary movements (e.g., linear/lateral displacement) in the relatively low-density vitreous, with no substantive progress toward either multimodal locomotion or responsive surgical maneuvers within the more demanding lens region.

Porcine eyes are frequently employed as model systems for human eyes due to anatomical similarities and comparable lens properties. Having characterized the microrobot's motion performance in viscoelastic media, we subsequently evaluated its operational capacity in ex vivo porcine lens models. Following continuous curvilinear capsulorhexis (CCC) procedures, helixbots were wirelessly actuated within the lens using magnetic fields with maintained optimal parameters (8 Hz frequency, 8 A/m amplitude) as previously established. Experimental results confirmed the robotic platform's capacity for omnidirectional navigation through the lens matrix, with handle-controlled actuation delivering sufficient force generation and precise velocity modulation for controlled mobility beneath the anterior capsule.

Throughout these experiments, we established cataract models in ex vivo porcine eyes using controlled microwave irradiation. By administering microwave exposure across graduated durations (0–7 seconds), we induced progressive protein denaturation to simulate sequential stages of lens opacification. We further deployed helixbots to execute fundamental nucleus chopping operations in porcine eyes exhibiting varying cataract severity. Figure 4A demonstrates that in microwave-untreated lenses, helixbots achieved linear propulsion through rotational screw motion while performing lens cutting operations that generated substantial groove depth. The straight arrows denote directional movement vectors whereas curved arrows indicate rotational states. As shown in Fig. 4B, after 3-second microwave exposure producing mild opacification, our helixbot surgical system effectively performed lens segmentation, creating characteristic elongated grooves analogous to clinical phacoemulsification patterns. Figure 4C documents the system's operational capacity in moderately opacified lenses (5-second exposure), where we observed progressively narrowing groove dimensions correlating with advancing cataract severity. Crucially, the helixbot surgical system consistently maintained core lens segmentation functionality despite these increasing operational challenges. When microwave exposure reached 7 seconds (severe opacification), helixbots exhibited markedly diminished cutting performance, managing only partial cortical tissue incision on the lens surface without achieving deep nuclear fragmentation grooves (Fig. 4D). The results presented in Figure S3 indicate that, in untreated porcine lenses, the movement speed of the helixbot was measured at 0.419 ± 0.226 mm/s. Following microwave treatment for exposure times of 3 seconds and 5 seconds, the cutting speeds of the helixbot on the lens decreased to 0.138 ± 0.083 mm/s and 0.012 ± 0.006 mm/s, respectively, demonstrating that as the degree of cataract increased, the cutting speed of the helixbot slowed down. After 7 seconds of microwave treatment, the helixbot could only move and advance within a viscoelastic medium, cutting

small portions of the cortex on the lens surface, with its movement speed slightly increasing to 0.832 ± 0.575 mm/s. Figure S4 provides enhanced visualization of helixbot cutting processes across cataract stages: substantial incision depth following 3-second (Fig.S4a) and 5-second (Fig.S4b) exposures versus exclusively superficial cortical cutting in severe cataract conditions (Fig.S4c). This performance limitation demonstrated direct correlation with elevated mechanical resistance in sclerotic lens tissue.

We also investigated the rotational characteristics of helixbots in lens tissues exhibiting varying cataract severity. Our experimental results confirm that in untreated porcine lenses and those with mild cataracts (3-second microwave exposure), helixbots successfully executed turns exceeding 180°(Fig.S5a-b). In contrast, lenses with moderate-to-severe cataracts showed significantly reduced turning angles, with maneuverability progressively constrained as lens nuclear hardness increased (Fig.S5c-d). Similarly, when manipulating helixbots to perform deeper incisions using downward-oriented helical modules, effective cutting depth was maintained in mild/moderate cataracts (Fig.S6a-b), whereas severe cataracts imposed mobility restrictions limiting cutting efficacy (Fig.S6c).

Through micro-robot-assisted cataract surgery, we observed the system's force modulation dynamically adapting to distinct biomechanical properties of the lens nucleus and capsule (Fig. 4E). The robotic system generates sufficient nuclear fragmentation forces while operating below the rupture threshold of more elastic capsular tissue. This controlled magnetic actuation enables selective tissue interaction, permitting safe lens fragmentation while preserving capsular integrity. Arrows in Fig. 4E identify the anterior capsule boundary after helixbot manipulation. These results demonstrate that our magnetically controlled micro-robot system significantly reduces iatrogenic tissue damage compared to conventional phacoemulsification, potentially lowering surgical complication rates.

The movement and operational results of the helixbot in ex vivo porcine lens models demonstrate that this microrobot can successfully perform several critical intra-capsular procedures under a composite magnetic drive system: in the light to moderate cataract models, it accomplished nuclear division and deep cutting through a helical propulsion mechanism, while exhibiting agile maneuverability in porcine eye models with varying degrees of opacity. Notably, no capsule damage or other complications were observed in any of the porcine eye samples operated on by the helixbot, confirming the safety of the surgical procedures. However, there are certain limitations to the helixbot’s operation in cataract eyes: in the severe cataract model, the operational efficiency of the helixbot declined; although it could displace the superficial cortex, effective cutting was difficult to achieve, and its rotation efficiency was also lower compared to the light to moderate cataract group. This phenomenon may be attributed to the helical cutting structure of the helixbot being 3D printed from resin material, which has relatively insufficient hardness, making it challenging to cut through the high-hardness nucleus of severely opaque cataracts. This suggests that the design of the robot may be better suited for surgical scenarios involving light to moderate cataracts.

The findings of this study validate the effectiveness and safety of using magnetic-controlled microrobots in lens surgery. However, even though the helixbot has demonstrated the ability to perform basic nuclear

division and some cutting operations, there is still a gap towards the goal of enabling the magnetic-controlled robot to complete the entire process of nuclear fragmentation. In the future, our research needs to focus on shortening the operational time of the robot by optimizing the dynamic parameters of the magnetic field and improving the morphological design of the robot to enhance its movement speed and tissue penetration power within the eye; furthermore, it is necessary to integrate a negative pressure suction system to facilitate the removal of fragmented lens material while maintaining anterior chamber stability, thereby establishing a comprehensive robotic-assisted process for cataract nucleus management.

This study proposes a novel cataract surgical system based on magnetic-controlled microrobots that introduces a new concept of robotic mechanical fragmentation without the need for ultrasonic energy intervention. Compared to traditional phacoemulsification, this microminiature robotic technology not only avoids ultrasonic energy-related damage but also allows for high-precision operations within the confined space of the lens, potentially significantly reducing the risk of postoperative complications. In the future, integrating autonomous navigation systems and surgical decision-making modules into robotic surgery, combined with visual closed-loop feedback for real-time adjustment of the robot's movement path, will enable the transformation of complex operations into standardized and automated processes, thereby reducing intraoperative complication rates and enhancing the safety of cataract patients. At the same time, this could lower the surgical learning curve, with the potential to promote advanced surgical techniques in grassroots medical settings. This work offers an innovative alternative to phacoemulsification, marking a significant step toward the evolution of ophthalmic surgery towards autonomous robotic microsurgical paradigms.

a Helixbot performing lens cutting in untreated tissue; **b** Lens cutting after 3-second microwave exposure; **c** Partial lens resection following 5-second microwave treatment. **d** Superficial cortical cutting post 7-second microwave exposure; **e** Helixbot executing screw-type precession and directional steering along the anterior capsule boundary.

3. Conclusion

In this study, we successfully developed a helixbot magnetic-controlled intraocular surgical system specifically designed for nucleus fragmentation during cataract surgery. After establishing a kinematic simulation model and computational framework for the motion of micro-nano robots within biological tissues, we utilized the developed electromagnetic-permanent magnet composite drive system to control the helixbot, enabling multi-modal motion exploration in a viscoelastic medium and in ex vivo porcine eye lenses through handle manipulation. In the viscoelastic medium, we assessed the propulsion and steering speeds of the helixbot under various magnetic field frequencies and amplitudes, providing valuable guidance for parameter selection in subsequent animal eye experiments. Additionally, we achieved autonomous route navigation for the helixbot within this viscoelastic environment. In experiments involving porcine eye lenses, we found that the helixbot could effectively perform lens cutting in cases of mild to moderate cataracts without causing complications such as damage or

rupture of the lens capsule. Although the cutting operations faced some limitations in cases of severe cataracts, this micro-robotic surgical system still shows promising potential for a safer approach to cataract nucleus fragmentation surgery that does not rely on ultrasonic energy, thus laying a solid foundation for the future development of robotic cataract surgery.

4. Experimental Section

Fabrication of the Microrobot

The helical microrobots were fabricated using stereolithography (SLA) technology. First, the helical substrates were precisely manufactured using an SLA 3D printer (Formlabs Inc., Somerville, MA, USA) with a biocompatible photopolymer resin (Dental SG Resin, Formlabs Inc., Somerville, MA, USA). Subsequently, a cylindrical axially magnetized permanent magnet (diameter: 1 mm; height: 1 mm) was uniformly coated with the aforementioned Dental SG Resin and cured under ultraviolet (UV) irradiation for 10 minutes to form a dense biocompatible encapsulation layer. Finally, the encapsulated magnet was assembled with the helical structure using the same resin as an adhesive. The assembly was subjected to in situ curing under UV irradiation for 10 minutes while strictly maintaining the alignment where the magnet's generatrix was perpendicular to the axis of the helical structure, thereby achieving a robust and integrated connection.

Integrated Human-Machine Interaction Platform

In high-viscosity solutions, the movement of the micro magnetic-driven robot is influenced by its weight and fluid resistance, necessitating a strong driving force. Unlike a rotating magnetic field, a gradient magnetic field can provide significant gradient forces, enabling the micro magnetic-driven robot to perform two-dimensional and even three-dimensional movements. Additionally, the magnetization direction of the micro magnetic-driven robot automatically aligns with the direction of the magnetic field. Currently, most micro robots rely on manual control, depending on the operator's experience and visual assessment to determine control accuracy. This method is unstable and has limited precision. Therefore, it is crucial to develop a closed-loop control system that can autonomously navigate based on image feedback:

$$\begin{cases} \dot{x}(t) = v_1\big(w(t)\big) + b(t) \\ \dot{y}(t) = v_2\big(w(t)\big) + b(t) \\ \dot{\alpha}(t) = \dot{\beta}(t) \end{cases} \tag{2.1}$$

$$\begin{bmatrix} v_1(w(t)) \\ v_2(w(t)) \end{bmatrix} = \begin{bmatrix} \cos(\emptyset(t)) & 0 \\ 0 & \sin(\emptyset(t)) \end{bmatrix} \begin{bmatrix} k(w(t)) \\ k(w(t)) \end{bmatrix} \tag{2.2}$$

To model the motion of the micro magnetic-driven robot, we employ a first-order model. In the equations (2.1 and 2.2) mentioned above, the ratio represents the instantaneous velocity of the robot or robot

cluster to the frequency of the externally applied magnetic field. External disturbances may exist in the environment, while represents the steering rate of the externally applied magnetic field input, and denotes the manipulation rate of the micro magnetic-driven robot or its group.

In automatic control mode, the controller adjusts the directional vector and control voltage based on the real-time positions of the magnetically controlled micro robots as captured by the two industrial cameras, following a pre-set trajectory. This enables precise three-dimensional trajectory control. This section will conduct corresponding experimental validations on the magnetic control system regarding the two-dimensional and two-dimensional trajectory control of the micro magnetic-driven robot. By integrating the Meanshift algorithm into the host computer program, we achieved real-time position capture of the robot, and the sliding mode controller reduced trajectory control errors, facilitating autonomous navigation trajectory control for the micro magnetic-driven robot.

Preparation of the lens and propulsion experiments under the microscope

Fresh porcine eyes were procured from a local abattoir on the morning of the experiment and maintained on ice until use. A LuxOR Revalia ophthalmic surgical microscope (Alcon Laboratories, USA) was employed to ensure a clear surgical field. To document the surgical procedure for subsequent analysis and facilitate precise incisions and capsulorrhexis, a surgical video recording system and software (Shenzhen Jinkangqiao Technology Co., Ltd, China) were utilized. Initially, the fresh porcine eye was stabilized using an ophthalmic surgical model to ensure immobility during the procedure. Following stabilization, a 3.2 mm clear corneal main incision was performed 2 mm posterior to the limbus using a microscopic corneal scissor, accompanied by auxiliary incisions at appropriate locations. A viscoelastic agent (1.7% sodium hyaluronate, Eyecare Company) was introduced into the anterior chamber to maintain its depth and protect the corneal endothelium. Subsequently, a continuous circular capsulorrhexis with an approximate diameter of 5.5 mm was meticulously executed using capsulorrhexis forceps (ASICO AE-4223), ensuring that the edges of the capsulotomy were smooth and continuous. Following the preparation of the anterior capsule, hydrodissection was performed using a balanced salt solution (BSS-I, Alcon, USA). This involved the insertion of a 26G blunt needle between the lens cortex and the nucleus, utilizing a layered injection technique to achieve complete separation of the nucleus from the cortex. To induce cataract formation in porcine eyes, an 800-watt microwave oven, operating at a frequency of 2450 Hz, was employed without pre-heating. Subsequently, a magnetically controlled helixbot was implanted into the lens, and the magnetic driving system was activated to facilitate the observation of the helixbot's motion and effects within the porcine eye lens.

Data analysis and statistics

All biological assays were repeated at least three times. The experimental data are presented as the mean ± standard deviation and assessed by Origin statistically. The quantitative data were compared by t-test or one-way analysis of variance (ANOVA) between different groups. The results were considered statistically significant if P-value < 0.05.

Declarations

Acknowledgements

This research was supported by the China Postdoctoral Science Foundation (No. 2025M772106) and the Science Research Foundation of Aier Eye Hospital Group (AMF2409D01). We would like to thank KHAN MUHAMMAD AHMAD, Jieli Wu and Yixiong Tang for their helpful discussions. No ethical approval was required in this case.

Author contributions

Z. L., and Y. W. contributed equally to this work. Z. L. and D. L. conceived the project. Z. L. and X. F. fabricated the helixbot and completed the tests. Z. L. and Y. W. conduct experiments in porcine eyes. Z. L., Y. W., Q. T., and W. S. performed data processing and analysis. Z. L., D. L. and X. F. co-wrote the paper. D. L. and X. F. supervised the project. All authors discussed the results and commented on the manuscript.

Data Availability Statement

The original contributions presented in the study are included in the article. Further inquiries can be directed to the corresponding authors.

Declaration of competing interest

The authors declare that they have no known competing financial interests or personal relationships that could have appeared to influence the work reported in this paper.

References

1. Chen, X., Xu, J., Chen, X. & Yao, K. Cataract: Advances in surgery and whether surgery remains the only treatment in future. *Adv Ophthalmol Pract Res* 1, 100008, doi:10.1016/j.aopr.2021.100008 (2021).
2. Cicinelli, M. V., Buchan, J. C., Nicholson, M., Varadaraj, V. & Khanna, R. C. Cataracts. *Lancet* 401, 377–389, doi:10.1016/S0140-6736(22)01839-6 (2023).
3. Yoshizaki, M. *et al.* How can we improve the quality of cataract services for all? A global scoping review. 49, 672–685 (2021).
4. Wyględowska-Promieńska, D., Jaworski, M., Kozieł, K., Packard, R. J. V. & Techniques, O. M. The evolution of the anterior capsulotomy. 14, 12–18 (2019).
5. Briceno-Lopez, C. *et al.* Corneal Edema after Cataract Surgery. *J Clin Med* 12, 6751, doi:10.3390/jcm12216751 (2023).
6. Chen, H. C. *et al.* Accelerated Corneal Endothelial Cell Loss after Phacoemulsification in Patients with Mildly Low Endothelial Cell Density. *J Clin Med* 10, 2270, doi:10.3390/jcm10112270 (2021).

7. Gajraj, M. & Mohan, A. Safety and efficacy of manual small-incision cataract surgery in patients with brunescent and black cataracts and other ocular comorbidities. *Indian J Ophthalmol* 70, 3898–3903, doi:10.4103/ijo.IJO_1565_22 (2022).
8. Deshmukh, R. & Vajpayee, R. B. Intraocular endothelial Keratogel Device for protection corneal endothelium during phacoemulsification cataract surgery. *Eye (Lond)* 39, 622–623, doi:10.1038/s41433-024-03518-y (2025).
9. Yamazaki, K. *et al.* Efficacy of femtosecond laser-assisted cataract surgery for cataracts due to atopic dermatitis. 12, 41–47 (2021).
10. Preetam, S. *et al.* Empowering tomorrow's medicine: energy-driven micro/nano-robots redefining biomedical applications. *Design & Engineering* 9, 892–911 (2024).
11. Chen, Y. *et al.* Recent advances in field-controlled micro–nano manipulations and micro–nano robots. 4, 2100116 (2022).
12. Sun, M. *et al.* Exploiting ferrofluidic wetting for miniature soft machines. *Nat Commun* 13, 7919, doi:10.1038/s41467-022-35646-y (2022).
13. Cheng, Q. *et al.* Magnetic Control Strategies of Microrobot Swarm for Biomedical Applications. *ACS Biomater Sci Eng* 11, 5264–5284, doi:10.1021/acsbiomaterials.5c01155 (2025).
14. Wang, T., Chen, Z., Huang, Q., Arai, T. & Liu, X. Advanced Microrobots Driven by Acoustic and Magnetic Fields for Biomedical Applications. *Cyborg Bionic Syst* 6, 0386, doi:10.34133/cbsystems.0386 (2025).
15. Chen, Y. *et al.* A soft micron accuracy robot design and clinical validation for retinal surgery. *Microsyst Nanoeng* 11, 170, doi:10.1038/s41378-025-01002-5 (2025).
16. Chen, B. *et al.* Visible-light-driven TiO2@ N-Au nanorobot penetrating the vitreous. 27, 101455 (2022).
17. Yu, J. *et al.* Active generation and magnetic actuation of microrobotic swarms in bio-fluids. *Nat Commun* 10, 5631, doi:10.1038/s41467-019-13576-6 (2019).

Figures

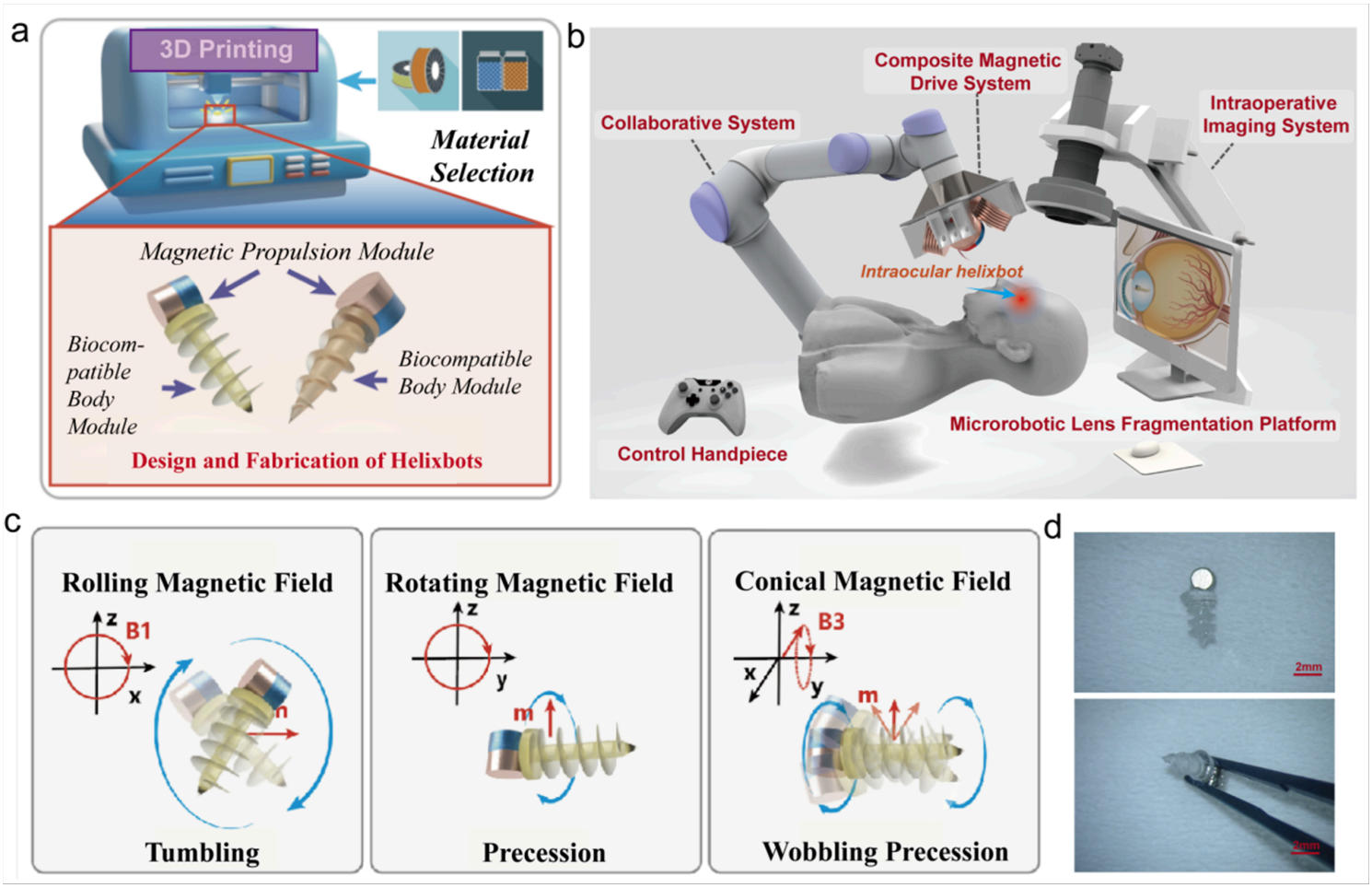


Figure 1

The concept, structure and mechanism of the helixbot surgery system designed for lens fragmentation. **a** Typical structure scheme for the helixbot system **b** Conceptual framework of the helixbot platform for lens nucleus fragmentation in human cataract surgery **c** Three magnetic field modes for controlling multimodal motion of the magnetically controlled helical microrobot **d** Microscopic characterization of the helixbot's appearance

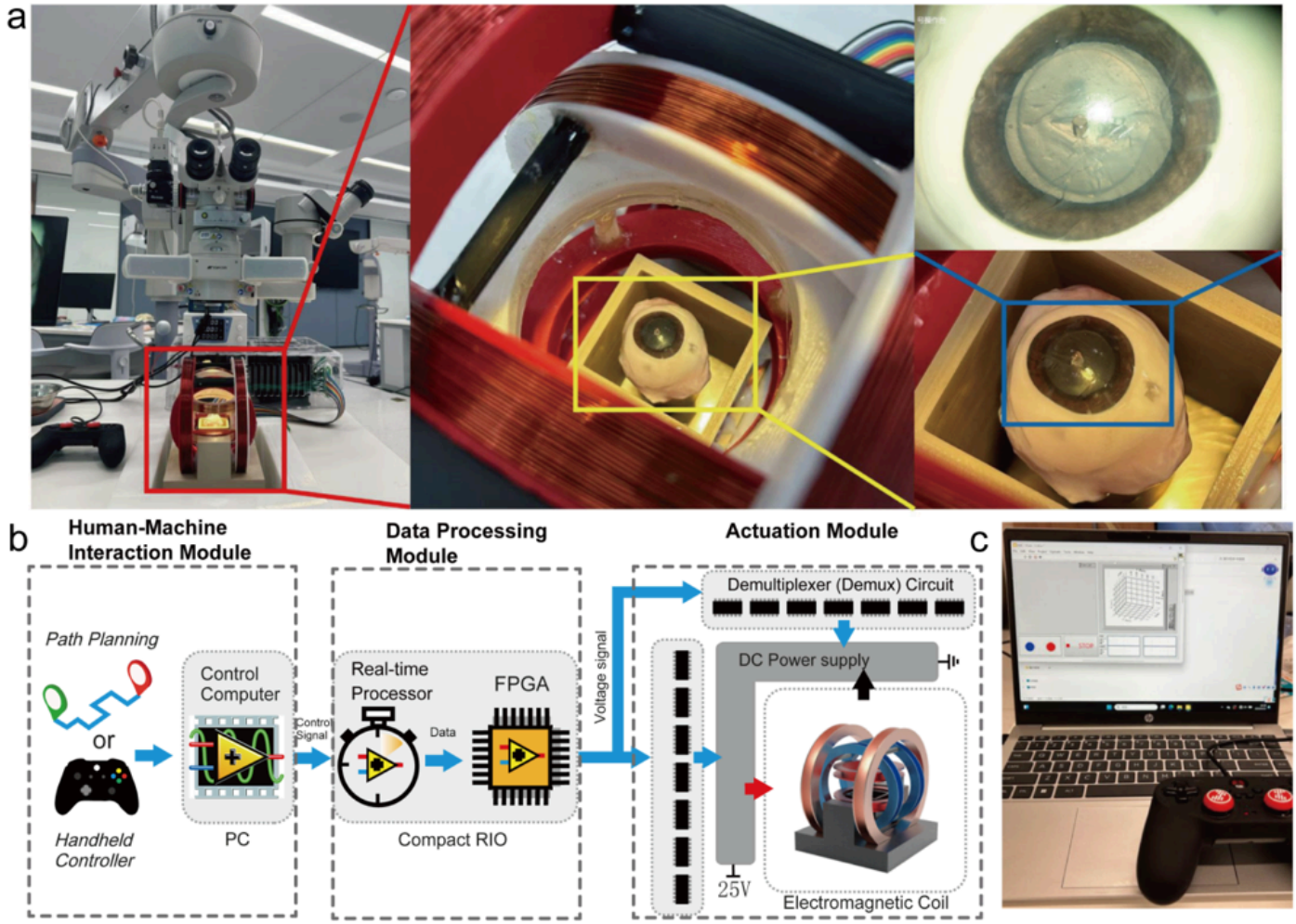


Figure 2

Design and Development of a Robotic Surgery System a Intraoperative view of porcine eye surgery under Topcon OMS-800 ophthalmic microscope (Fixed fresh porcine eye positioned centrally within the magnetic actuation system, with microrobot deployed in the lens region)**b** Schematic diagram of human-machine interaction, data processing, and operational execution modules**c** LabVIEW control interface and handheld manipulator

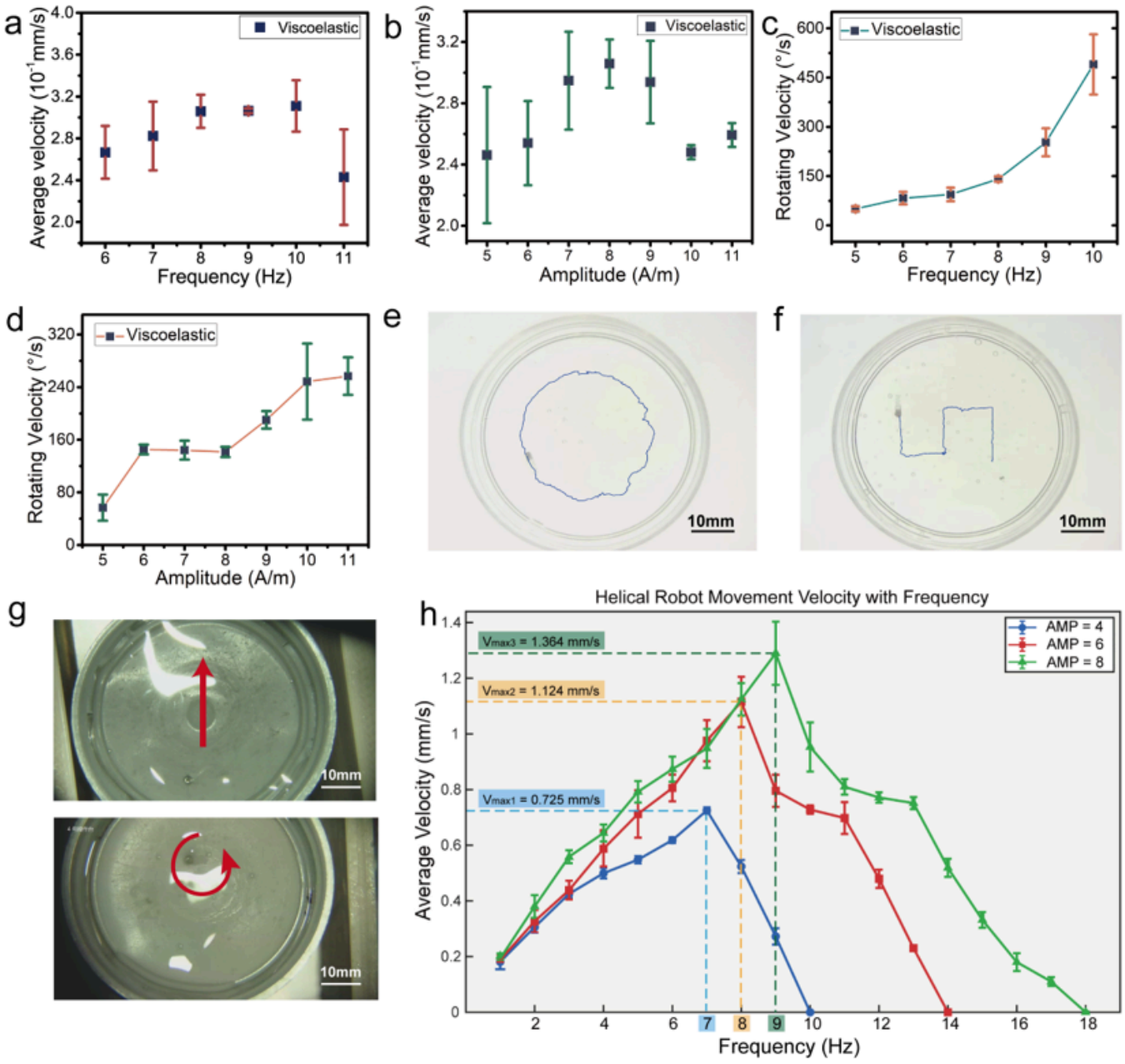


Figure 3

Fig. 2. Characterization of in vitro controllable motion of Helixbot **a** Propulsion velocity versus magnetic field frequency in viscoelastic environment; **b** Propulsion velocity versus magnetic field amplitude in viscoelastic environment; **c**Rotational velocity versus magnetic field frequency in viscoelastic environment; **d** Rotational velocity versus magnetic field amplitude in viscoelastic environment; **e** Circular trajectory under autonomous navigation; **f** Linear trajectory under autonomous navigation; **g**Motion performance within viscoelastic environment; **h** Velocity dependence on frequency and amplitude during autonomous navigation.

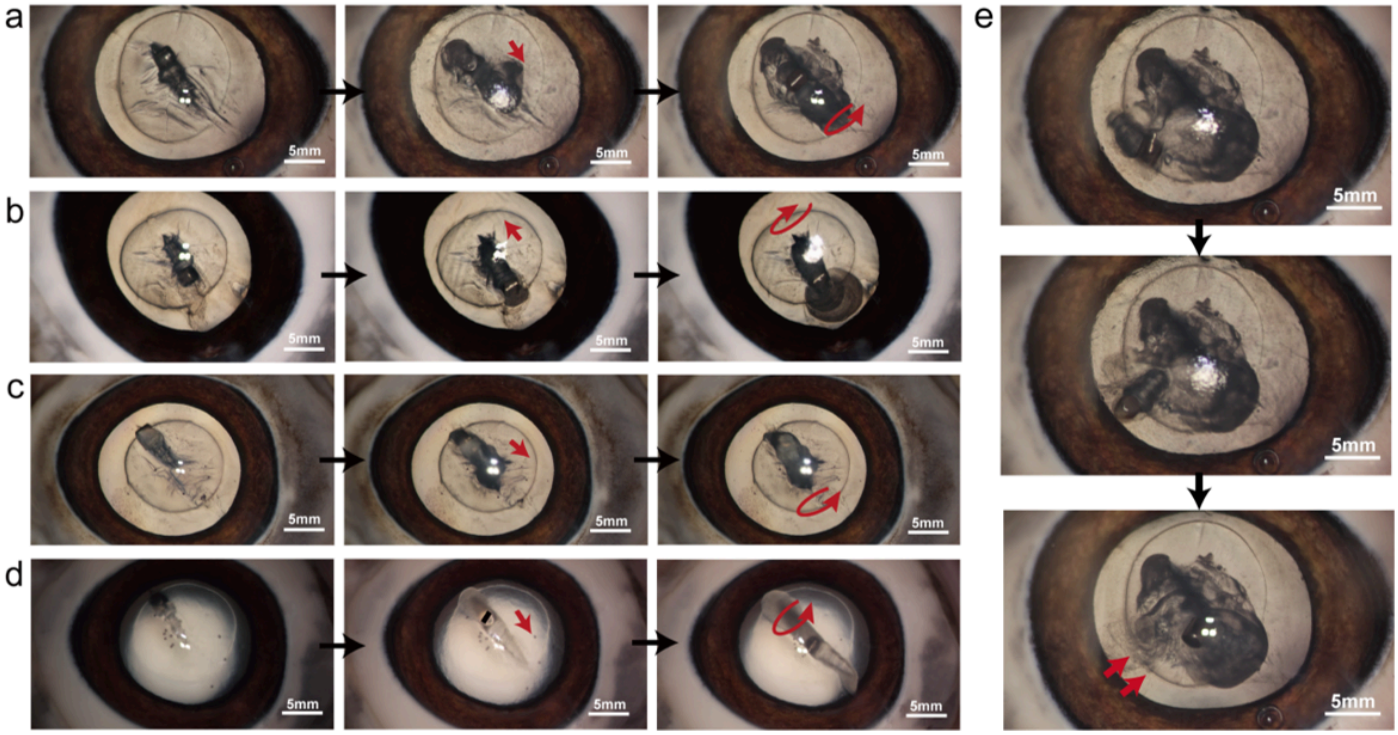


Figure 4

Fig. 4. Magnetically controlled helixbot locomotion within porcine lenses.a Helixbot performing lens cutting in untreated tissue; **b** Lens cutting after 3-second microwave exposure; **c** Partial lens resection following 5-second microwave treatment. **d** Superficial cortical cutting post 7-second microwave exposure; **e** Helixbot executing screw-type precession and directional steering along the anterior capsule boundary.

Supplementary Files

This is a list of supplementary files associated with this preprint. Click to download.

- MovieS1.mp4
- MovieS2.mp4
- MovieS3.mp4
- MovieS5.mp4
- MovieS4.mp4
- SIinformation.docx